Applied Catalysis B: Environmental 221 (2018) 691–700

Contents lists available at ScienceDirect

Applied Catalysis B: Environmental

journal homepage: www.elsevier.com/locate/apcatb

Research Paper

Degradation of azo dye Orange II under dark ambient conditions by calcium strontium copper perovskite

Huihuang Chen[a], Julius Motuzas[a], Wayde Martens[b], João C. Diniz da Costa[a,*]

[a] The University of Queensland, FIM²Lab – Functional Interfacial Materials and Membranes Laboratory, School of Chemical Engineering, Brisbane, Qld 4072, Australia
[b] Science and Engineering Faculty, Queensland University of Technology, Brisbane, Qld 4000, Australia

ARTICLE INFO

Keywords:
Dark conditions
Orange II degradation
Perovskite
Heterogeneous catalysis

ABSTRACT

This work investigates the effect of calcium strontium copper (CSC) based catalysts for the degradation of an azo dye orange II (OII) under dark conditions without the addition of peroxides or ozone. CSC were synthesized via a combined EDTA-citric acid complexation method. The resultant catalyst was composed of perovskite and metal oxide phases, however, the perovskite phase was the most active for degradation of OII. The content of Ca and Sr in the A-site of the perovskite structure was varied whilst the B-site was Cu rich. CSC compounds with higher Ca content in the A-site were slightly more effective at degrading OII. The degradation kinetics under dark conditions was fast with up to 80% of OII being degraded within 10 min. TOC results showed that the degradation was only partial as more than 60% of the organic carbon remained in the solution, supported by the formation of by-products determined by HPLC. The remainder of the carbon were found to be adsorbed on the surface of the spent CSC catalyst, as by-products of the reaction and OII molecules. The CSC catalyst proved to be effective for breaking −N=N− bonds from solutions containing low (10 ppm) to high (100 ppm) OII concentrations. This reaction produced electrons which generated radical species, including hydroxyl radicals as confirmed by 2-propanol, which further degraded OII and its by-products.

1. Introduction

The disposal of wastewaters containing organic pollutants from textile industries is of global environmental concern. Worldwide approximately 280,000 tons of textile dyes are discharged in industrial effluents every year [1,2]. Azo dyes, which contain −N=N− bonds, are widely used by the textile industries, accounting for over 50% of all commercial dyes [3]. These dyes are non-biodegradable and toxic [4–6], whilst affecting water transparency even at small concentrations (1 ppm L^{-1}) [7], limiting the penetration of sunlight necessary for aquatic photosynthesis [8]. For this reason, textile wastewater emissions have been scrutinised by non-governmental agencies and the public resulting in environmental protection agencies around the world developing stringent guidelines to control their emissions and have legislated hefty penalties for non-compliance. To address this problem, many processes based on physical, biological and chemical methods, have been developed and trialled. In general, physical methods (e.g. flocculation, adsorption and membrane filtration) suffer from secondary pollution as they merely transfer pollutants downstream without achieving a real degradation of target pollutants [9]. As such, physical processes still require downstream processing of wastewaters. Bio-treatment of azo dyes is usually considered ineffective due to the resistance of the dyes to aerobic degradation [10,11]. Biodegradation requires the use of living organisms under strict process conditions (e.g., pH and temperature) [12] which tend to be greatly affected in textile wastewaters due to the toxicity of most commercial dyes [13]. Additionally, azo dyes undergo reductive cleavage through anaerobic biological treatment and potentially generate toxic aromatic amines [14,15].

Advanced oxidation processes (AOPs), in which highly reactive oxidative species (e.g. HO·, $O_2\cdot^-$, O_2, HOO· and HO_2· [16]) are utilized, have been widely studied as an alternative way of treating organic pollutants [17]. AOPs can be categorized into photo- and dark-oxidation procedures. Photocatalysis, especially using TiO_2 catalysts, is widely known as an efficient method to remove and destroy organic pollutants under light irradiation. For instance, Cd-doped TiO_2 degraded 95% of OII after 2 h when illuminated with visible light [18]. Photocatalysis however is generally energy intensive and greatly inhibited in the absence of light illumination. Dark oxidation (e.g., ozonation, ultrasonication and Fenton process) are alternative methods, dispensing the need of light radiation, by requiring reactants such as O_3 and/or H_2O_2. The heterogeneous Fenton-like reaction has proved to be

* Corresponding author.
E-mail address: j.dacosta@uq.edu.au (J.C. Diniz da Costa).

http://dx.doi.org/10.1016/j.apcatb.2017.09.056
Received 26 April 2017; Received in revised form 13 September 2017; Accepted 25 September 2017
Available online 27 September 2017
0926-3373/

attractive, with the production of new catalysts such as iron oxides compounded with graphene oxide [19], Cu sulfate [20], and vanadium titanate [21]. Compounds containing graphene oxide have been found to greatly improve the degradation efficiency of OII, though Cu sulfate iron oxide proved to deliver the best performance reaching ~100% OII degradation in 60 min. These reactions do however need H_2O_2 to generate the powerful HO· radicals for the destruction of organics. A more interesting approach is the degradation of organic pollutants in wastewaters without the aid of external stimulants or light illumination. In this way, there is no need for extra costs associated with the consumption of chemical products or energy.

Recently, perovskites have attracted the attention of the research community due to their ability to oxidize and remove organic compounds from wastewater in dark ambient conditions. Perovskites are crystalline ceramics with a cubic structure described by the general formula ABO_3, where the partial substitution of the cation sites (A or B) with other cations (A' or B') results in $A_xA'_{1-x}B_yB'_{1-y}O_{3-\delta}$ compounds. Rummino et al. [22] showed that $Sr_{0.85}Ce_{0.15}FeO_{3-\delta}$ perovskite-type mixed oxide degraded orange II and rhodamine B as model pollutants without light irradiation. Initial reports using $BaFeO_{3-\delta}$ showed it took 5 days to remove 50% of methyl orange [23]. By replacing Ba in the A-site with Sr and forming a perovskite $SrFeO_{3-\delta}$, acid orange 8 (150 μM) was degraded in 60 min [24]. These results give a clear indication that the cation used in the perovskite compound plays a major role in the catalytic degradation of organics in wastewaters. There are a number of cations that can be used as doping rare earth or earth alkaline elements at the A site and transitional metals at the B site. A transitional metal of interest is Cu, with recent reports for oxygen systems showing outstanding performance in $Ba_{0.5}Sr_{0.5}Co_{0.8}Cu_{0.2}O_{3-\delta}$ (BSCC) [25], or in binary $Co_{0.8}Cu_{0.2}O_x$ [26] compounds. Indeed, Cu has been used as a cation in perovskite compounds and tested for the degradation of organic compounds in solutions. However, these Cu containing perovskites were tested using hydrogen peroxide in a heterogeneous Fenton-like reaction. Examples include Cu doped $LaTiO_3$ perovskite for the degradation of rhodamine B [27] and $LaCuO_3$ perovskite for the degradation of phenol [28].

Therefore, this work investigates the performance of novel perovskites in the degradation of dyes under dark conditions and without any external stimulants (i.e. no ozone or no hydrogen peroxide). We fully substituted Fe in the B-site with Cu, and in the A-site Sr was partially or fully substitute with Ca, in a series of $Ca_xSr_{1-x}CuO_{3-\delta}$ (CSC) with x varying from 0, 0.25, 0.5, 0.75 to 1. OII dye was the model organic pollutant tested as it is widely used in the textile industry. The CSC perovskites were fully characterized to understand their materials properties; and tested from low (10 ppm) to high (100 ppm) OII aqueous concentrations. The relationship between the materials properties and catalytic performance is discussed and an OII degradation mechanism using CSC perovskite under dark condition is proposed.

2. Materials and methods

2.1. Synthesis and characterisation

All chemicals were used as received including strontium nitrate (98% Alfa Aesar), copper (II) nitrate hemi (pentahydrate) (98% Alfa Aesar), calcium nitrate tetrahydrate (> 99.0% Chem-Supply Pty Ltd), aqueous ammonia solution (30% Chem-Supply Pty Ltd), citric acid monohydrate (99.5% Chem-Supply Pty Ltd) and ethylenediamine tetraacetic acid (EDTA, 99% Sigma-Aldrich). The target organic pollutant was OII also known as Acid Orange 7 (Molecular formula: $C_{16}H_{11}N_2NaO_4S$, M_w:350.32 g mol^{-1}, λ_{max} = 485 nm, > 85% Sigma-Aldrich).

CSC ($Ca_xSr_{1-x}CuO_{3-\delta}$, x = 0, 0.25, 0.5, 0.75 and 1) was prepared via a combined EDTA-citric acid complexation method. The molar ratios of total metal ions, EDTA, citric acid, and ammonium hydroxide were kept at 1:1.1:2:10. Initially, ammonia aqueous solution was added to a beaker containing EDTA under stirring until EDTA was completely dissolved and a clear solution was formed. In a separate beaker, stoichiometric quantities of nitrate salts and citric acid were dissolved in deionized water to obtain a mixture solution. Subsequently, the EDTA solution was added into the mixture solution under stirring to get the desired solution, which was heated while magnetically stirred to evaporate most water until a viscous fluid was attained. This final mixture was initially sintered in atmospheric air in a furnace up to 450 °C with a dwell time of 8 h utilizing heating and cooling rates of 5 °C min^{-1}. A second sintering step was applied up to 1000 °C using the same dwell time and ramping rates.

The crystalline phase of the ground samples was characterized by X-ray powder diffraction (XRD, D8 Advance, Bruker, USA) with Cu-Kα radiation (λ = 1.5406 Å) at 40 kV and 40 mA by step scanning in the range of 10° ≤ 2θ ≤ 100°. X-ray photoelectron spectroscopy (XPS) was performed on X-ray photoelectron spectrometer (Kratos Axis ULTRA) equipped with monochromatic Al Kα (hv = 1486.6 eV) radiation and calibrated internally by carbon deposit C 1s binding energy (BE) at 284.8 eV to quantitatively analyse the chemical composition of samples and chemical state of elements. The powder morphology was analysed using a scanning electron microscope (SEM) equipped with an energy dispersive X-ray spectroscopy (EDS). Nitrogen adsorption at 77.4 K on degassed samples at 150 °C was carried out using a Micromeritics TriStar 3000 to determine BET surface area. The remaining TOC in the sample solutions was monitored using a Shimadzu TOC-Vcsh Total Organic Carbon Analyzer. Mass loss analysis was performed using a TGA-DSC 1 Thermogravimetric Analyser (Mettler Toledo) by heating the samples from 28 to 800 °C at a heating rate of 5 °C min^{-1} under air atmosphere at a flow rate of 80 mL min^{-1}. The infrared absorption spectra were recorded using a Fourier transform infrared (FTIR) spectrophotometer (IRAffinity-1, Shimadzu).

2.2. Catalyst evaluation

The catalytic degradation of OII over dispersed CSC was conducted in a 250 mL beaker, in which 200 mg of the catalyst was suspended in 200 mL of OII aqueous solution in dark at room temperature without any external stimulant. The dispersion of CSC in water was achieved by magnetic stirring during the degradation process. At designated intervals, ~5 mL of reaction suspension was sampled and filtered using 0.45 μm Milipore syringe filters. The samples were analysed using a UV–vis spectrophotometer (Evolution 220, Thermo Fisher Scientific) to determine the degradation yield (d) of OII at its characteristic wavelength $d = (A_0–A_t)/A_0$, where A_t is the absorbance of treated OII solution at time t and A_0 is the absorbance of the initial OII solution. Recyclability of CSC was evaluated using OII (20 ppm). At the time interval of 15 min, 5 mL reaction mixture was sampled and analysed by UV–vis spectrometer. After each cycle (1 h reaction), 20 mL 2000 ppm OII stock solution was added to the remaining reaction mixture (180 mL) to compensate the consumed OII and to maintain the 200 mL reaction mixture volume. 2-propanol (Alfa Aesar, 0.10 M) mixed in an OII solution was used as hydroxyl radical (HO·) scavenger.

A fully computer controlled HPLC system (UltiMate 3000, UHPLC$^+$ focused, Thermmo Scientific) comprising a quaternary solvent delivery pump, diode array and fluorescence detectors and an auto sampler was used to follow OII concentration-time profiles. Potential products were separated on an Eclipse XDB-C8 5 μm, 150 mm × 4.6 mm column using 70:30 aqueous solution of ammonium acetate (20 mM): acetonitrile as an isocratic mobile phase at 1 mL min^{-1} and ambient temperature. The injection volume was 20 μL and detection was achieved with the diode array detector set at 253 nm. Degradation products were determined using liquid chromatography-mass spectrometry (LC–MS) system. A LC system (UltiMate 3000, UHPLC$^+$ focused, Thermmo Scientific) was equipped with a C18 column (4.6 mm × 150 mm × 5 μm) and coupled online to an electrospray ionisation mass spectrometer (ESI–MS, Thermo Fisher Scientific Orbitrap Elite).

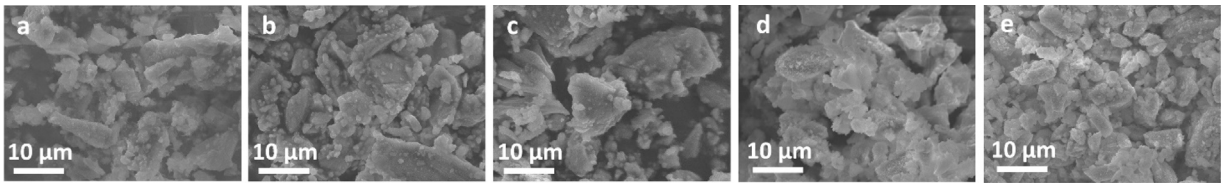

Fig. 1. SEM images of CSC for x values of (a) 0, (b) 0.25, (c) 0.5, (d) 0.75 and (e) 1.0.

3. Results and discussion

3.1. Catalyst characterization

Fig. 1 shows the representative SEM images of CSC samples. It is observed that all samples are composed of non-homogeneous particles of differing sizes. Particle sizes ranged from less than 1 µm to as large as 10 µm. Many of the smaller particles are interconnected via necks to large particles, an effect of the sintering temperature up to 1000 °C. It is also noted a number of irregular shaped pores with sizes varying up to 10 µm. The pores tend to be small and well packed in the case of smaller particles, whilst large pores are observed between larger particles. BET surface analyses (see Appendix Fig. A1) indicates that all these samples are essentially constituted of dense solid particles with similar surface area of $\sim 0.3\ m^2\ g^{-1}$.

Fig. 2 displays the XRD patterns of all CSC samples containing perovskites structures in addition to single metal oxides. The XRD patterns allocate to perovskites display peaks similar to $Ca_{0.3}Sr_{0.7}CuO_2$ and $Ca_5Sr_9Cu_{24}O_{41}$ (JCPDS PDF # 48-0140 and 48–1501, respectively). The CSC samples are characterized by crystal phases with orthorhombic unit cells. In the case of CSC (x = 0) the most intense peaks at 2θ 25.16, 25.45, 29.75, 31.61, 32.85, 34.35, 37.23, 37.82, 44.07, 44.30, 46.41, 50.32, 51.05 and 52.26 were attributed to a strontium copper oxide phase (PDF2#01-083-0266). Also observed are low intensity peaks at 2θ 26.95, 28.43, 30.71, 38.15 and 42.33 assigned to strontium hydroxide (PDF2#01-071-2365), whilst minor phases with peaks at 2θ 30.71, 31.05 and 33.35 ascribed to strontium copper oxide (PDF2#00-048-1496). As the amount of Ca increases in the ternary metal oxides CSC ($0.25 \leq x \leq 0.75$), a CSC perovskite phase (PDF2#00-048-1506) at 2θ 16.92, 21.65, 24.88, 25.693, 30.02, 31.46, 32.73, 34.04, 37.11, 37.75, 43.98, 46.00, 46.30, 51.38 and 52.05 became prominent. It is also interesting to note that as the Ca content increases, the peaks with the highest intensities start shifting to higher 2θ angles. The equimolar A-site mixture (x = 0.5) exhibits two crystalline CSC phases, a major (PDF2#00-048-1509) and a secondary (PDF2#01-085-2489) phase.

Further increase in calcium to x = 0.75 resulted in the formation of CaO at 2θ 31.77, 36.91 and 52.78 as the major phase (PDF2#01-070-5490). Further, a secondary phases appeared at 2θ 14.37, 27.83, 31.84, 34.42, 35.58, 43.425, 45.386, 46.28, 46.99 and 54.65 for a perovskite $Ca_{1.6}Sr_{0.4}CuO_3$ (PDF2#00-048-1482) compound and at 2θ 17.87, 33.62 and 49.9 for calcium hydroxide (PDF2#00-044-1481). Finally, the samples containing calcium and copper only (x = 1) were composed by three major phases: calcium copper oxide (PDF2#00-034-0282) at 2θ 14.49, 35.24, 44.39, 46.38, 47.38, 48.14 and 56.45, calcium oxide (01-070-4068) at 2θ 31.77, 36.91, 52.78 and copper (I) oxide (PDF2#01-071-3645) at 2θ 36.44, 42.32 and 61.42. Small amounts of calcium hydroxide (PDF2#00-044-1481) at 2θ 32.29, 37.36 and 53.93; and Copper (II) oxide (PDF2#01-073-6023) at 2θ 35.67 and 38.92 were also observed in the XRD pattern. All these results clearly indicate that a complex compound was formed and that the CSC samples contain a mixture of perovskites, metal oxides and metal hydroxides.

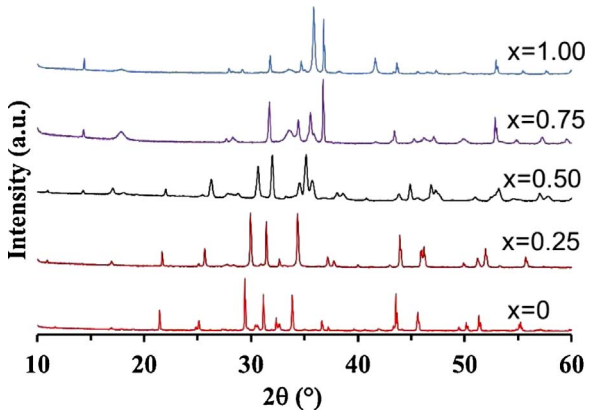

Fig. 2. XRD patterns of CSC samples.

3.2. Catalyst performance

The degradation of OII was initially studied by varying the cation concentration $Ca_xSr_{1-x}CuO_{3-\delta}$ in the A-site ($0 \leq x \leq 1$). Fig. 3a shows that all compositions were very effective in a fast degradation of OII solution of 50 ppm. Similar performance was also observed for processing OII solutions of 10 and 100 ppm (see Appendix Fig. A2). The CSC samples containing a higher amount of Ca (x = 0.75 and 1) in Fig. 3a gave the best results with ~80% degradation in 10 min, and ~95% in 60 min. It is interesting that this rapid degradation was achieved under dark conditions without the addition of ozone or peroxide. The samples containing high amounts of Sr (x = 0 and 0.25) also gave fast initial sharp degradation though reaching a maximum OII degradation efficiency of ~90% at 60 min. The performance of the equimolar sample (x = 0.5) was similar to the Sr rich samples. In principle, these results indicate that Ca in the A-site of the CSC structure was more active for the degradation of OII under dark conditions. Long term stability testing in Fig. 3b shows that the CSC sample first cycle of 85% OII degradation efficiency reduced in subsequent cycles and became stable at ~75% from cycle 5.

However, the XRD patterns showed that the CSC compounds are actually complex mixtures of perovskite, metal oxides and hydroxides. In order to verify which phases are the most active, the degradation of OII was carried out for single and mixed metal oxides. Table 1 displays the concentration of OII after 120 min. The single and mixed metal oxides showed OII degradation up to 50%. Subsequently, we acidified the degraded solutions with 0.5 M HCl and found that the OII concentration increased to $0.63 \geq C/C_o \geq 0.87$. This is related to the pH effect of OII in the solution which affects the OII absorbance intensity measure at 485 nm. Interestingly, the subsequent acidification of OII solutions tested using CSC samples showed small to almost non-existent changes in the OII concentration. Therefore, these results strongly suggest that the active phase in CSC compound is the perovskite phase. Further, the OII aqueous solution without any catalyst was also tested, showing no degradation (Appendix - Fig. A3). Therefore, the OII degradation is solely attributed to the catalytic properties of CSC compound.

Although the CSC perovskite phase is the most active, it is interesting that the samples containing Ca (x = 0.75 and 1) were more active in the degradation of OII (Fig. 3a). Further analyses of the XRD patterns (Fig. 2) clearly indicate a major difference between CSC samples. The samples with high Sr content (x = 0 and 0.25) were made mainly of a major perovskite phase with minor oxide phase. In contrast,

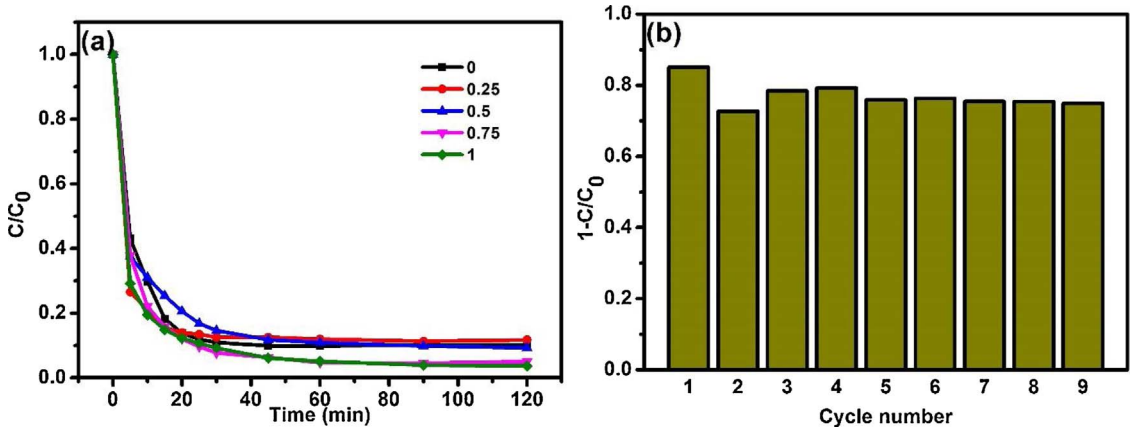

Fig. 3. (a) Effect of Ca and Sr cation concentration in the A-site of CSC for the degradation (± 2 ppm) of OII. Experimental conditions: $[OII]_0$ = 50 ppm, magnetic stirring, RT, dark. (b) Cycling stability of CSC (x = 0.75) sample. Experimental conditions: $[OII]_0$ = 20 ppm, magnetic stirring, RT, dark.

Table 1
OII concentration using single and mixed metal oxides, and CSC samples. Experimental conditions: $[OII]_0$ = 10 ppm, catalyst dosage = 1 g L^{-1}, magnetic stirring, RT.

Samples	2h	2h + acid
CaO	0.52	0.84
SrO	0.58	0.73
CuO	0.69	0.79
CaO + SrO	0.61	0.87
CaO + CuO	0.48	0.67
SrO + CuO	0.47	0.63
CaO + SrO + CuO	0.50	0.71
CSC (x = 0)	0.19	0.27
CSC (x = 0.25)	0.26	0.30
CSC (x = 0.5)	0.16	0.24
CSC (x = 0.75)	0.16	0.16
CSC (x = 1)	0.14	0.14

the samples with a high amount of Ca (x = 0.75 and 1) had two major phases of perovskite and oxides, in addition to hydroxides. Therefore, the improved performance of the CSC samples with high Ca content could be attributed to a compounding effect of double oxides and pH. In the first instance, the presence of CaCuO resulted in 0.86 of OII degradation (Table 1), thus aiding in the overall performance. This type of effect has also been observed for CaNiO for the degradation of methylene blue using visible light [29]. The pH effect is also contributory as calcium oxide has a propensity to form calcium hydroxide in aqueous solution, thus increasing the pH. The pH of the samples containing Ca were slightly higher than those containing Sr (see Appendix Fig. A4). This is in line with reports for the degradation of indigo carmine using calcium oxide and visible light, where degradation efficiency increased from 95.4% for pH 9–10 to 100% for pH 12 [30].

The OII solutions were decolorized during testing, given a clear indication of the destruction of azo bond N=N [31]. OII exists in two tautomeric forms in equilibrium aqueous solution [32] and the hydrazone form is predominant in aqueous solution [33,34]. The UV–vis spectrum of OII solution in the visible region in Fig. 4a exhibits two main bands at 430 and 485 nm, corresponding to transition of the azo and hydrazone forms, in addition to two other peaks at 230 and 310 nm assigned to the benzene and naphthalene rings of OII molecules [35]. Fig. 4a also shows the UV–vis absorption evolution of OII degradation as a function of time. The initial band for OII is the base line at time 0 min. Within the first 5 min, all bands significantly decreased, whilst almost disappearing at 20 min. This confirms the OII degradation rates in Fig. 3 at 50 ppm. Simultaneously, two new bands started to appear at 254 and 344 nm which can be attributed to byproducts. In order to confirm the presence of byproducts, TOC analyses in Fig. 4b clearly indicates that the degradation of OII was partial, as more than 64% of carbon remained in the solution after 120 min. Of interest, it is noted that the samples containing a higher concentration of Sr (CSC x = 0 and 0.25) had the lowest TOC readings, whilst the equimolar sample (CSC x = 0.5) was almost ineffective in degrading OII with a TOC reading as high as 92%.

In order to understand further the by-product formation observed in the UV–vis spectra in Fig. 4a, a HPLC analysis was carried out of OII solutions degraded to 120 min. The resulting chromatograms and UV–vis spectra are presented in Fig. 5a and b, respectively. The chromatogram of OII (sample at time 0 min) has a major peak at retention times (t_R) 2.5 min and a minor peak at 2.02 min. The analysis of the solution after 1 min treatment revealed that the peaks corresponding to initial OII remained almost the same though at lower intensity. This clearly indicates that OII degradation occurred very quickly in the first min of reaction. There is also a minor peak appearing at 1.3 min. As the reaction proceeds further to 5 and 120 min, the OII major peak at 2.5 min retention time reduces significantly in intensity, while the new peak at 1.3 min retention time slightly increases in intensity as seen in the UV–vis spectra (Fig. 5b). These results confirm the breakdown of OII molecules and the generation of by-products which were further analysed by LC–MS technique. Table 2 lists a number of smaller molecular by-products formed during the degradation of OII.

3.3. Role of CSC compounds and reaction mechanism

The surface chemistry of the CSC catalysts was analyzed by XPS in order to understand the structural evolution prior and after catalytic testing. The survey XPS spectra (see Appendix Fig. A5) indicate that the surface of pristine and spent CSC were composed of Ca, Sr, Cu, O and adventitious C. High resolution spectra were deconvoluted as displayed in Fig. 6. The Ca 2p XPS narrow spectrum in Fig. 6a shows double peaks at 346.8 eV and 350.3 eV attributed to Ca 2p3/2 and Ca 2p1/2 components, respectively [36]. The XPS narrow spectrum for the Sr 3d (Fig. 6b) with peaks at 133.2 and 135.3 eV corresponds to Sr^{2+} [37]. The Cu $2p_{3/2}$ peak at ~933.8 eV in Fig. 6c is accompanied by two satellites at ~941.8 to ~944 eV, which are assigned to Cu^{2+}, and the peak at ~932.8 eV to Cu^{1+} [38]. Considering the relative intensity of Cu 2p spectra for both pristine and spent catalyst, Cu presented mainly as Cu^{2+} in both samples. This clearly indicates that oxidation of Cu was not significantly affected as is the case with Fe in the Fenton reaction.

The binding energy of O 1s electrons in oxygen bonded to metal cations is one of the most informative parameters with respect to the oxide structure [39]. The O 1s oxygen spectra were deconvoluted into three distinguishable peaks (Fig. 6d). The peak at ~533 eV was attributed to trace amount of oxygen coming from carbonates [40]. The two peaks at the binding energies of ~531 eV and ~529 were assigned to adsorbed and lattice oxygen atoms, respectively [41,42]. The O 1 s

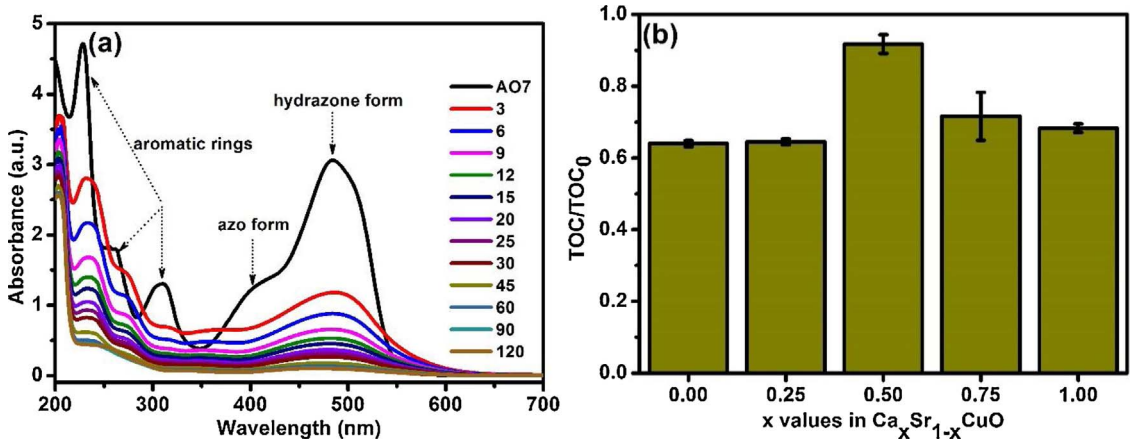

Fig. 4. (a) UV–vis absorption spectra evolution of OII with time and (b) TOC readings for CSC ($0 \leq x \leq 1$). Experimental conditions: $[OII]_0$ = 50 ppm, catalyst dosage = 1 g L^{-1}, magnetic stirring, RT.

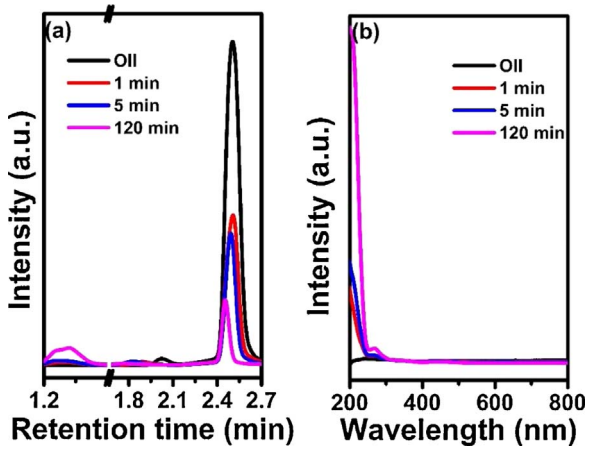

Fig. 5. (a) HPLC chromatograms and (b) UV–vis spectra of species found with reaction times of 0, 1, 5 and 120 min. Experimental conditions: $[OII]_0$ = 50 ppm, catalyst dosage = 1 g L^{-1}, magnetic stirring, RT.

Table 2
Reaction product ions identified from OII degradation.

Ion Number	*m/z* $[M\text{-}H]^-$	Elemental formula (ion)
1	200.98	$C_7H_5SO_5^-$
2	191.04	$C_{10}H_7O_4^-$
3	121.03	$C_7H_5O_2^-$
4	165.02	$C_8H_5O_4^-$
5	172.01	$C_6H_6NO_3S^-$
6	172.99	$C_6H_5O_4S^-$
7	157.00	$C_6H_5O_3S^-$
8	173.02	$C_{10}H_5O_3^-$
9	327.04	$C_{16}H_{11}N_2O_4S^-$

peak at ~529 eV was very similar for both pristine and spent catalyst, implying no changes in the lattice oxygen. However, the intensity of adsorbed oxygen at ~531 eV increased after the OII degradation process. This result indicates that oxygen containing species (O or OH) were present on the spent CSC surface which are derived from the catalytic process or from the formation of metal hydroxides as determined by XRD patterns (Fig. 2).

Under the testing conditions in a heterogeneous catalytic reaction, mass transfer of OII as the reactant from the fluid phase to contact the surface of the solid CSC catalyst was facilitated by the constant stirring of the solution. Upon contact, the reactant adsorbed on the surface of the solid catalyst followed by reaction as represented by Eqs. (1) and (2) below, respectively. TOC results (Fig. 4b) clearly indicate that the majority of carbon (~70%) remained in the solution after 120 min testing. Although the catalyst proved to be very efficient for OII degradation based on UV–vis measurements (Figs. 3 a and 4 a), the fate of 30% carbon needs to be ascertained if this was in fact attributed to partial mineralization or adsorption.

The TGA results in Fig. 7 show that the blank CSC sample (exposed to water for 2 h) resembles the pristine CSC sample, though it shows a higher mass loss. This was attributed to the hydroxylation of metal oxides (i.e. $CaO + H_2O \rightarrow Ca(OH)_2$) as the pristine CSC sample was not exposed to water. The spent and blank CSC samples have similar patterns up to 260 °C, where the mass loss of the spent CSC sample became higher than the blank CSC sample all the way to 550 °C. The final mass loss difference between the blank and spent CSC sample is ~2% per gram, equivalent to 20 mg. As the spent CSC sample was tested for a concentration of 50 ppm and 30% could not be accounted for as per TOC results, which is equivalent to 15 ppm or 15 mg. Within the experimental error of this work, in addition to the hydroxylation of metal oxides which may be slightly different in both blank and spent CSC, these results strongly suggest that the non-accounted 30% TOC value was definitely due to adsorption. However, the spent CSC sample mass loss profile differs from the OII profile, thus given a clear indication that other compounds were adsorbed on the surface of the CSC catalyst after the reaction.

In order to further understand the adsorption of compounds on the CSC catalyst, the FTIR results in Fig. 8 show that the spent CSC samples has several minor intensity peaks which can be correlated to the major intensity peaks in the spectrum of OII. At the same time, the pristine and spent CSC samples spectra resemble each other though the slightly broader doublet band 1454 and 1424 cm^{-1} [43] increased in intensity for the spent sample, together with the absorption band at 870 cm^{-1}. These bands are assigned to carbonates, indicating the increase in carbonate formation during reaction. The spectrum of the spent CSC sample was also compared to the spectra of the physically mixed OII (10 and 50 ppm) with pristine CSC. However, the spectrum of the spent CSC sample does not entirely resemble the spectra of the physically mixed samples. It is observed that the intensities at 1232 and 1253 cm^{-1} (linked to chromophore parts (i.e., −N−N− and −C−N−) of hydrazone form of OII, respectively) [44,45] are negligible compared with physical mixture of the pristine CSC + OII (10 ppm). Furthermore, the intensities of nearly all peaks (1450, 1553, 1568, 1596 and 1620 cm^{-1}) attributed to C=C aromatic skeletal vibrations [46] also decreased. Considering that the non-accounted 30% carbon from the TOC results are attributed to adsorption, equivalent to 15 ppm in the spent CSC sample, these results may suggest the adsorption of OII was lower than 10 ppm, and that other compounds derived from the reaction as by products also adsorbed on the surface of the spent CSC

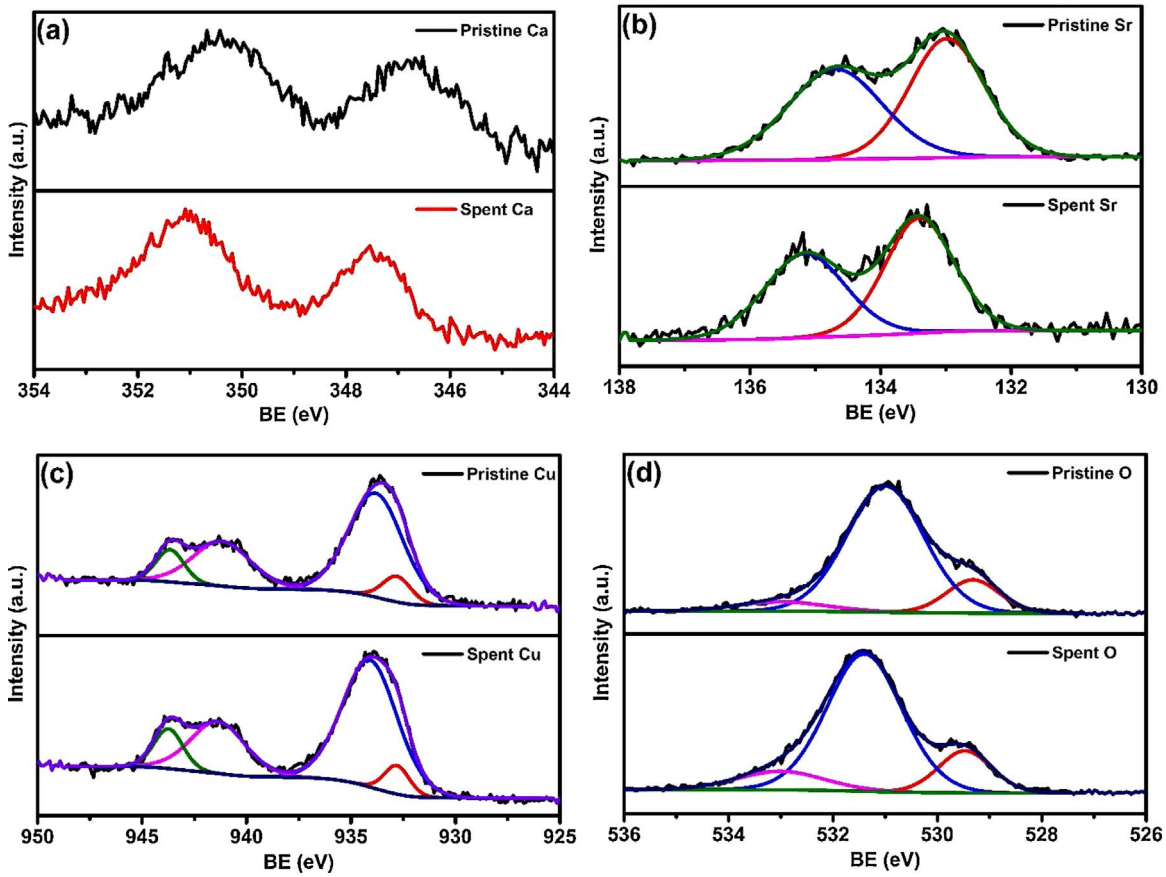

Fig. 6. Pristine and spent CSC high resolution XPS spectra of (a) Ca, (b) Sr, (c) Cu and (d) O.

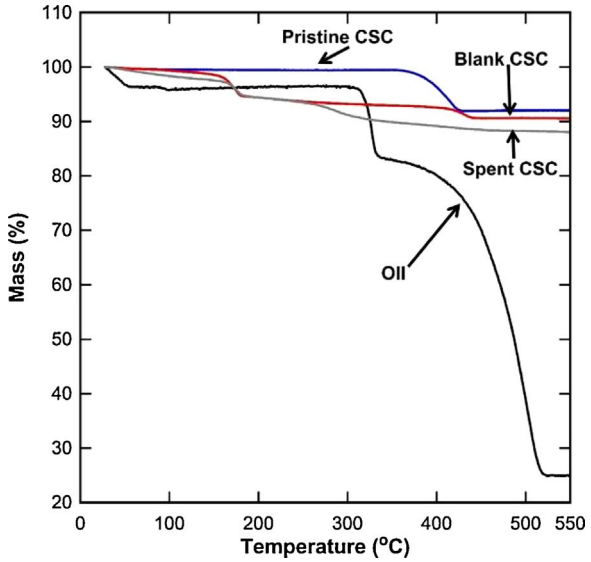

Fig. 7. TGA mass loss curves of OII, pristine CSC, blank CSC (water only) and spent CSC (50 ppm of OII) samples.

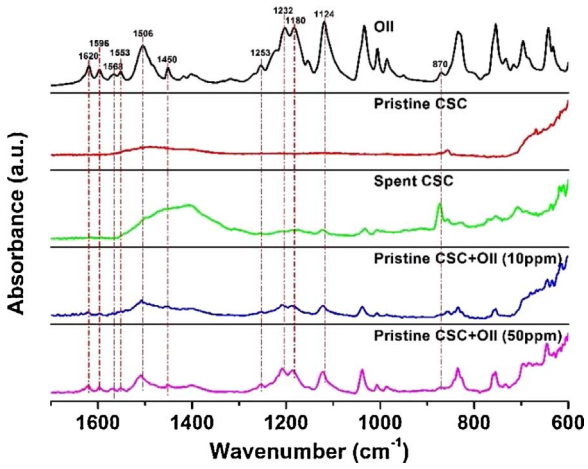

Fig. 8. FTIR spectra of OII, pristine CSC, spent CSC (50 ppm of OII) and physically mixed samples of OII (10 and 50 ppm) with pristine CSC (see Appendix Table A1 for band assignments).

sample.

As the tested solution was clear after testing, these results strongly suggest that the CSC catalyst was effective in breaking the conjugation in the OII molecules, particularly the −N=N− bonds, which are the most labile [47]. The breakdown of −N=N− bonds generate electrons (Eq. (2)). The perovskite phase of the complex CSC compound was ascertained to be the most active phase in the degradation of OII. As several by-products were formed as determined by HPLC (Fig. 5) and LC–MS (Table 2) measurements, then the fate of electrons in this reaction must be ascertained. Perovskites have good electron conductivity [48], particularly Cu, which is an electron conducting material. Therefore, to accept electrons CSC must also donate electrons to maintain electrical neutrality. The electrons generated in this reaction have the propensity to form superoxide radical anion $O_2^{\cdot-}$(Eq. (3)) in aqueous solutions. This process may have led to further reactions such as the generation of hydroperoxyl radical $HO_2^{\cdot}$ (Eq. (4)), which further reacted to obtain H_2O_2 (Eq. (5)), HO· and OH^-(Eq. (6)). Recently, Turmino et al. [22] reported the presence of hydroxyl radical species

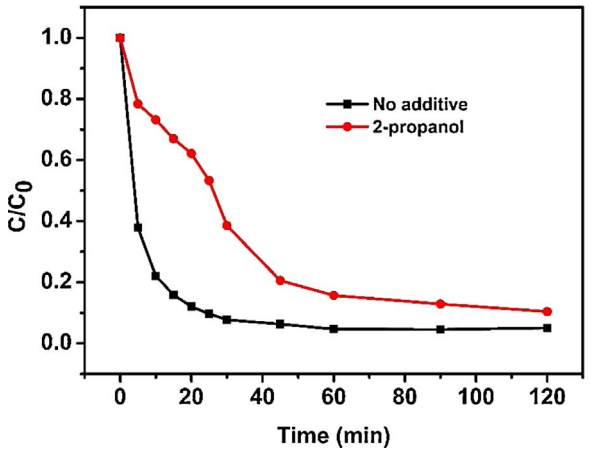

Fig. 9. Degradation curves of OII (50 ppm) with no additive and OII (50 ppm) plus 2-propanol (0.1 M) using CSC catalyst. Experimental conditions: [CSC] = 1 g L^{-1}, magnetic stirring, RT and dark.

(HO·) by using 2-propanol as a radical scavenger in the degradation of OII under dark conditions and using SrCeFe perovskites.

To confirm the presence of hydroxyl radicals in this work, 2-propanol was mixed with OII to make a solution prior to adding the CSC catalyst. Fig. 9 shows a reduction in the OII degradation for the mixture containing 2-isopropanol as compared to the OII solution without additives. These results confirm that hydroxyl radicals were generated, thus explaining the formation of several by-products. Further, the hydroxyl radicals can react with OII/OII^+ to generate a series of by-products (Eq. (7)). However, the hydroxyl radicals can be formed only when there is the supply of electrons by the breaking down of the azo bonds (Eq. (2)). Once this reaction is completed, then the supply of electrons ceased and likewise the generation of hydroxyl radicals.

$$OII + CSC \rightarrow CSC(OII) \quad (1)$$

$$CSC(OII) \leftrightarrow CSC + OII^+ + e^- \quad (2)$$

$$e^- + O_2 \rightarrow O_2^{\cdot-} \quad (3)$$

$$O_2^{\cdot-} + H^+ \leftrightarrow HO_2^{\cdot} \quad (4)$$

$$2HO_2^{\cdot} \rightarrow H_2O_2 + O_2 \quad (5)$$

$$H_2O_2 + e^- \rightarrow HO\cdot + OH^- \quad (6)$$

$$HO\cdot + OII/OII^+ \rightarrow \ldots \rightarrow by\ products \quad (7)$$

Appendix A

4. Conclusions

CSC compounds contained a complex structure of perovskite and metal oxide phases. These compounds were very effective in breaking down an azo dye molecule OII under dark ambient condition from low 10 ppm to high 100 ppm concentrations. Samples containing a higher content of Ca showed slightly higher degradation than those containing a high content of St in the A-site of the perovskite structure. The CSC catalyst proved to reach long term stability after 9 cycles of testing. Further, the perovskite phase of the CSC compound was more active in the degradation of OII than metal oxides.

The reaction kinetics were very fast, and within 60 min more than 82% of OII was degraded. However, the degradation was characterized by the breakdown of −N═N− bonds evidenced by clear solutions instead of reddish-yellow solutions containing OII. The degradation of OII was partial only, leading to formation of by-products as ascertained by HPLC and LC–MS. TOC accounted for more than 60% of the carbon, whilst the remainder of the carbon was found to be adsorbed on the surface of the spent CSC catalyst. The CSC compound delivered a combined catalytic effect under dark conditions, by effectively breaking down OII molecules whilst partially adsorbing by-products of the reaction and OII molecules. The surface of the CSC catalyst was very active, thus reacting with OII and generating by-products and electrons. The electrons played a major role in the formation of hydroxyl radicals, which further degraded OII and/or its by-products. Once the breakdown of −N═N− bonds ceased, then the reaction reached completion, the supply of electrons stopped and hydroxyl radicals were no longer generated.

Acknowledgements

H. Chen gratefully acknowledges for the China Scholarship Council and The University of Queensland scholarships. Authors thank the Australian Research Council (ARC) financial support (FT130100405). J.C. Diniz da Costa thanks the support from the ARC via the Future Fellowship Program (FT130100405).

Table A1
Orange II FT-IR bands assignment.

Wavenumber (cm-1)	Assignment	Ref.
870	CO2-3/CO_2/H_2O	[43]
1124	ν_s(SO-1 3)	[49]
1180	ν_{as}(SO-1 3)	[49]
1232	ν(N−N) (hydrazone)	[44,45]
1253	ν(C−N) (hydrazone)	[44,45]
1429–1454	−N═N−	[50]
1452	−N═N-	[51]
1500	−N═N−[a]	[52]
1500	−N−H (hydrozone from)	[49]
1506	δ(N−H)	[8,9]
1553	ν(C═N) + δ(N−H)	[53]
1622	ν(C═C) aromatic + ν(C═N)	[45]

[a] Or an aromatic ═C═C− vibration which is sensitive to the azo bond.

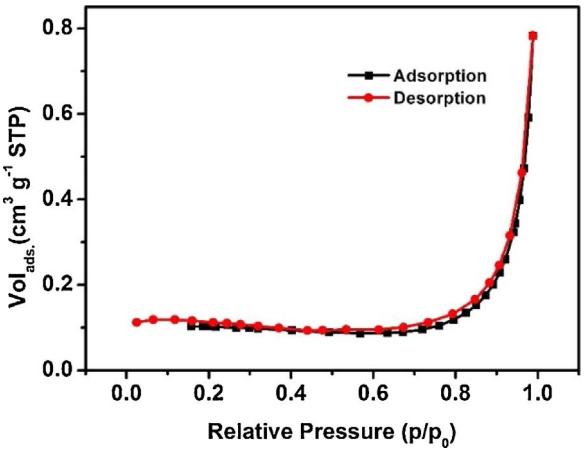

Fig. A1. Representative nitrogen sorption isotherm of CSC samples (x = 0.75). This isotherm of Type II, is characteristic of dense particles due to the very low adsorbed volume at low relative pressures. The increase of volume at $p/p_o > 0.75$ is associated with the inter-particle space.

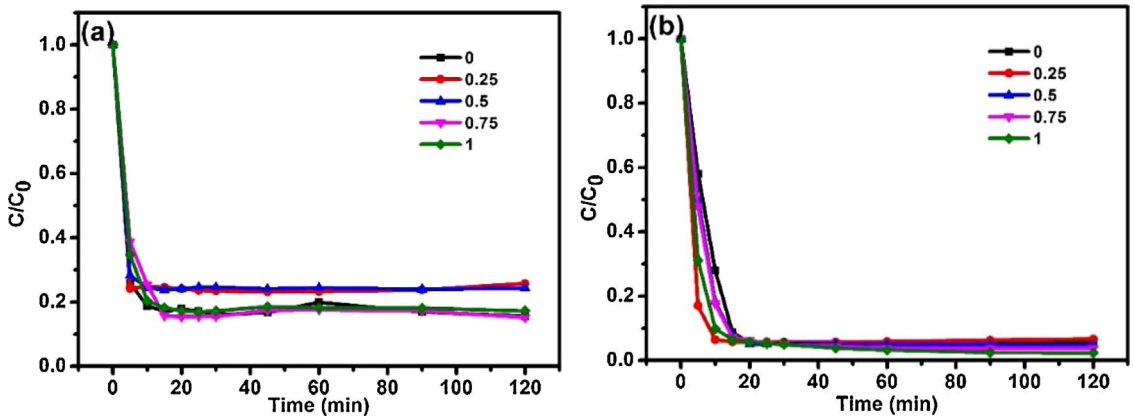

Fig. A2. Effect of Ca and Sr cation concentration in the A-site of CSC for the degradation (± 2 ppm) of OII for $[OII]_0$ of (a) 10 ppm and (b) 100 ppm. Experimental conditions magnetic stirring, RT and dark.

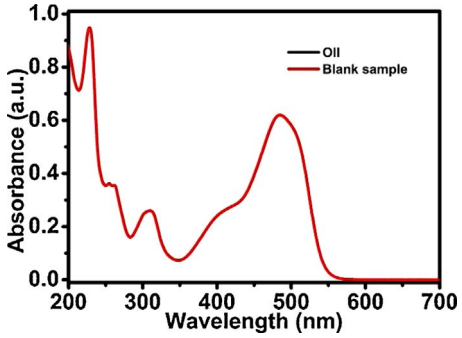

Fig. A3. Degradation of OII (10 ppm) without any catalyst after 120 min. Experimental conditions: magnetic stirring, RT, dark.

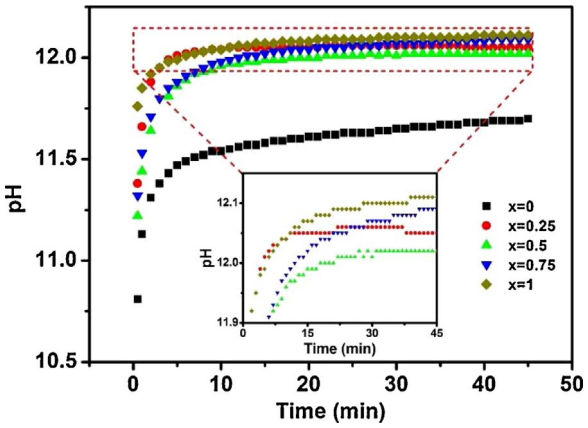

Fig. A4. pH measured as a function of time during the degradation of OII.

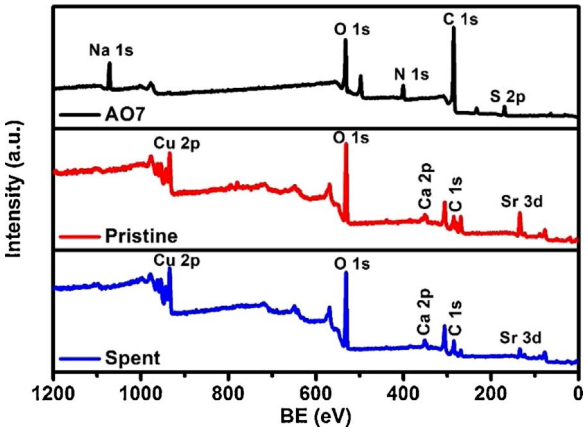

Fig. A5. Survey XPS spectra of OII, pristine and spent CSC.

References

[1] R. Maas, S. Chaudhari, Adsorption and biological decolourization of azo dye Reactive Red 2 in semicontinuous anaerobic reactors, Proc. Biochem. 40 (2005) 699–705.

[2] E. Brillas, C.A. Martínez-Huitle, Decontamination of wastewaters containing synthetic organic dyes by electrochemical methods. An updated review, Appl. Catal. B Environ. 166 (2015) 603–643.

[3] A. López-López, J. Pic, H. Debellefontaine, Ozonation of azo dye in a semi-batch reactor: a determination of the molecular and radical contributions, Chemosphere 66 (2007) 2120–2126.

[4] R.V. Khandare, A.N. Kabra, A.A. Kadam, S.P. Govindwar, Treatment of dye containing wastewaters by a developed lab scale phytoreactor and enhancement of its efficacy by bacterial augmentation, Int. Biodet. Biodegrad. 78 (2013) 89–97.

[5] J. Wang, C. Liu, J. Li, R. Luo, X. Hu, X. Sun, J. Shen, W. Han, L. Wang, In-situ incorporation of iron-copper bimetallic particles in electrospun carbon nanofibers as an efficient Fenton catalyst, Appl. Catal. B Environ. 207 (2017) 316–325.

[6] S. Garcia-Segura, E. Brillas, Combustion of textile monoazo, diazo and triazo dyes by solar photoelectro-Fenton: decolorization, kinetics and degradation routes, Appl. Catal. B Environ. 181 (2016) 681–691.

[7] S. Wijetunga, X.-F. Li, C. Jian, Effect of organic load on decolourization of textile wastewater containing acid dyes in upflow anaerobic sludge blanket reactor, J. Hazard. Mater. 177 (2010) 792–798.

[8] R. Kant, Textile dyeing industry an environmental hazard, Natural Sci. 4 (2012) 22.

[9] X. Lu, B. Yang, J. Chen, R. Sun, Treatment of wastewater containing azo dye reactive brilliant red X-3B using sequential ozonation and upflow biological aerated filter process, J.Hazard Mater. 161 (2009) 241–245.

[10] U. Pagga, D. Brown, The degradation of dyestuffs: part II Behaviour of dyestuffs in aerobic biodegradation tests, Chemosphere 15 (1986) 479–491.

[11] D. Brown, P. Laboureur, The degradation of dyestuffs: part I primary biodegradation under anaerobic conditions, Chemosphere 12 (1983) 397–404.

[12] C. Fernández, M.S. Larrechi, M.P. Callao, An analytical overview of processes for removing organic dyes from wastewater effluents, Trends Anal. Chem. 29 (2010) 1202–1211.

[13] S. Raghu, C.W. Lee, S. Chellammal, S. Palanichamy, C.A. Basha, Evaluation of electrochemical oxidation techniques for degradation of dye effluents—a comparative approach, J. Hazard. Mater. 171 (2009) 748–754.

[14] K.-T. Chung, C.E. Cerniglia, Mutagenicity of azo dyes: structure-activity relationships, Mutation Res. Rev. Genetic Toxicol. 277 (1992) 201–220.

[15] R. Anliker, Ecotoxicological assessment of dyes with particular reference to ETAD's activities, J. Soc. Dyers Colourists 95 (1979) 317–326.

[16] M. Antonopoulou, E. Evgenidou, D. Lambropoulou, I. Konstantinou, A review on advanced oxidation processes for the removal of taste and odor compounds from aqueous media, Water Res. 53 (2014) 215–234.

[17] M.A. Oturan, J.-J. Aaron, Advanced oxidation processes in water/wastewater treatment: principles and applications. A review, Cri. Rev. Environ. Sci. Technol. 44 (2014) 2577–2641.

[18] P. Margan, M. Haghighi, Hydrothermal-assisted sol–gel synthesis of Cd-doped TiO_2 nanophotocatalyst for removal of acid orange from wastewater, J. Sol-Gel Sci. Technol. 81 (2016) 1–14.

[19] N.A. Zubir, C. Yacou, J. Motuzas, X. Zhang, X.S. Zhao, J.C. Diniz da Costa, The sacrificial role of graphene oxide in stabilising Fenton-like catalyst GO–Fe_3O_4, Chem. Commun. 51 (2015) 9291–9293.

[20] J. Zheng, Z. Gao, H. He, S. Yang, C. Sun, Efficient degradation of Acid Orange 7 in aqueous solution by iron ore tailing Fenton-like process, Chemosphere 150 (2016) 40–48.

[21] X. Liang, Y. Zhong, S. Zhu, J. Zhu, P. Yuan, H. He, J. Zhang, The decolorization of Acid Orange II in non-homogeneous Fenton reaction catalyzed by natural vanadium–titanium magnetite, J. Hazard Mater. 181 (2010) 112–120.

[22] M.L. Tummino, E. Laurenti, F. Deganello, A.B. Prevot, G. Magnacca, Revisiting the catalytic activity of a doped $SrFeO_3$ for water pollutants removal: effect of light and temperature, Appl. Catal. B Environ. 207 (2017) 174–181.

[23] M. Sun, Y. Jiang, F. Li, M. Xia, B. Xue, D. Liu, Structure, dye degradation activity and stability of oxygen defective $BaFeO_{3-x}$, Mater. Trans. 51 (2010) 1981–1989.

[24] M.Y. Leiw, G.H. Guai, X. Wang, M.S. Tse, C.M. Ng, O.K. Tan, Dark ambient degradation of Bisphenol A and Acid Orange 8 as organic pollutants by perovskite SrFeO 3-δ metal oxide, J. Hazard Mater. 260 (2013) 1–8.

[25] A. Leo, J. Motuzas, C. Yacou, S. Liu, J.M. Serra, L. Navarrete, J. Drennan, A. Julbe, J.C. Diniz da Costa, Copper oxide – perovskite mixed matrix membranes delivering very high oxygen fluxes, J. Membr. Sci. 526 (2017) 323–333.
[26] J. Motuzas, J.C. Diniz da Costa, High performance oxygen production by CuCo binary oxides, J. Mater. Chem. A 3 (2015) 17344–17350.
[27] L. Zhang, Y. Nie, C. Hu, J. Qu, Enhanced Fenton degradation of rhodamine B over nanoscaled Cu-doped $LaTiO_3$ perovskite, Appl. Catal. B Environ. 125 (2012) 418–424.
[28] O.P. Taran, A.B. Ayusheev, O.L. Ogorodnikova, I.P. Prosvirin, L.A. Isupova, V.N. Parmon, Perovskite-like catalysts $LaBO_3$ (B = Cu, Fe Mn, Co, Ni) for wet peroxide oxidation of phenol, Appl. Catal. B Environ. 180 (2016) 86–93.
[29] L. Song, S. Zhang, A simple mechanical mixing method for the preparation of visible-light-sensitive NiO-CaO composite photocatalysts with high photocatalytic activity, J. Hazard. Mater. 174 (2010) 563–566.
[30] K.D. Veeranna, M.T. Lakshamaiah, R.T. Narayan, Photocatalytic degradation of indigo carmine dye using calcium oxide, Int. J. Photochem. 2014 (2014) 530570, http://dx.doi.org/10.1155/2014/530570.
[31] N. Deng, F. Luo, F. Wu, M. Xiao, X. Wu, Discoloration of aqueous reactive dye solutions in the UV/Fe^{o} system, Water Res. 34 (2000) 2408–2411.
[32] M. Stylidi, D.I. Kondarides, X.E. Verykios, Visible light-induced photocatalytic degradation of Acid Orange 7 in aqueous TiO_2 suspensions, Appl. Catal. B: Environ. 47 (2004) 189–201.
[33] E. Ember, S. Rothbart, R. Puchta, R. van Eldik, Metal ion-catalyzed oxidative degradation of orange II by H2O2 – high catalytic activity of simple manganese salts, New J. Chem. 33 (2009) 34–49.
[34] T. Hihara, Y. Okada, Z. Morita, Azo-hydrazone tautomerism of phenylazonaphthol sulfonates and their analysis using the semiempirical molecular orbital PM5 method, Dyes Pigm. 59 (2003) 25–41.
[35] H. Park, W. Choi, Visible light and Fe (III)-mediated degradation of Acid Orange 7 in the absence of H_2O_2, J. Photochem. Photobiol. A: Chem. 159 (2003) 241–247.
[36] M.L. Granados, M.Z. Poves, D.M. Alonso, R. Mariscal, F.C. Galisteo, R. Moreno-Tost, J. Santamaría, J. Fierro, Biodiesel from sunflower oil by using activated calcium oxide, Appl. Catal. B: Environ. 73 (2007) 317–326.
[37] X. Zhao, Q. Yang, J. Cui, XPS study of surface absorbed oxygen of ABO_3 mixed oxides, J. Rare Earth 26 (2008) 511–514.
[38] Z. Sroubek, Topics in surface and depth profile analysis, Spectrochim. Acta B At. Spectrosc. 44 (1989) 317–328.
[39] A. Mekki, XPS study of lead vanadate glasses, Arabian J. Sci. Eng. 28 (2003) 73–86.
[40] K. Yu, S. Yang, S.A. Boyd, H. Chen, C. Sun, Efficient degradation of organic dyes by $BiAg_xO_y$, J. Hazard. Mater. 197 (2011) 88–96.
[41] V. Dimitrov, T. Komatsu, Classification of simple oxides: a polarizability approach, J. Solid State Chem. 163 (2002) 100–112.
[42] F. López-Suárez, A. Bueno-López, M. Illán-Gómez, A. Adamski, B. Ura, J. Trawczynski, Copper catalysts for soot oxidation: alumina versus perovskite supports, Environ. Sci. Technol. 42 (2008) 7670–7675.
[43] J.T. Kloprogge, D. Wharton, L. Hickey, R.L. Frost, Infrared and raman study of interlayer anions CO32–, NO3–, SO42– and ClO4– in Mg/Al-hydrotalcite, Am. Mineral 87 (2002) 623–629.
[44] Y. Saito, B.-K. Kim, K. Machida, T. Uno, Resonace raman spectra of acid-base indicators. II. hydroxyarylazobenzene derivatives, Bull. Chem. Soc. Jpn. 47 (1974) 2111–2114.
[45] J. Kelemen, S. Moss, H. Sauter, T. Winkler, Azo—hydrazone tautomerism in azo dyes. II. Raman, NMR and mass spectrometric investigations of 1-phenylazo-2-naphthylamine and 1-phenylazo-2-naphthol derivatives, Dyes Pigm. 3 (1982) 27–47.
[46] P. Ji, J. Zhang, F. Chen, M. Anpo, Study of adsorption and degradation of acid orange 7 on the surface of CeO2 under visible light irradiation, Appl. Catal. B Environ. 85 (2009) 148–154.
[47] A.R. Khataee, M.R. Pons, O. Zahraa, Photocatalytic degradation of three azo dyes using immobilized TiO_2 nanoparticles on glass plates activated by UV light irradiation: influence of dye molecular structure, J. Hazard. Mater. 168 (2009) 451–457.
[48] H.J. Kim, U. Kim, T.H. Kim, J. Kim, H.M. Kim, B.-G. Jeon, W.-J. Lee, H.S. Mun, K.T. Hong, J. Yu, Physical properties of transparent perovskite oxides (Ba La) SnO_3 with high electrical mobility at room temperature, Phys. Rev. B 86 (2012) 165205.
[49] C. Bauer, P. Jacques, A. Kalt, Investigation of the interaction between a sulfonated azo dye (AO7) and a TiO_2 surface, Chem. Phys. Lett. 307 (1999) 397–406.
[50] R. Sperline, Y. Song, H. Freiser, Fourier transform infrared attenuated total reflection linear dichroism study of sodium dodecylbenzenesulfonate adsorption at the alumina/water interface using Al2O3-coated optics, Langmuir 10 (1994) 37–44.
[51] D. Peak, R.G. Ford, D.L. Sparks, An in situ ATR-FTIR investigation of sulfate bonding mechanisms on goethite, J. Colloid Interf. Sci. 218 (1999) 289–299.
[52] K. Vinodgopal, D.E. Wynkoop, P.V. Kamat, Environmental photochemistry on semiconductor surfaces: photosensitized degradation of a textile azo dye, acid orange 7 on TiO_2 particles using visible light, Environ. Sci. Technol. 30 (1996) 1660–1666.
[53] J.A. Connor, D.J. Fine, R. Price, Studies of chelation. Part 9. Cobalt complexes of 1-[(substituted phenyl) azo]-2-naphthol and 1-[(substituted phenylimino) methyl]-2-naphthol ligands. Tautomerism and reactivity, J. Chem. Soc. Dalton Transac. 2 (1981) 559–566.